Role of Pulse Phase and Direction in Two-Dimensional Optical Spectroscopy

ARTICLE *in* THE JOURNAL OF PHYSICAL CHEMISTRY A · NOVEMBER 1999

Impact Factor: 2.69 · DOI: 10.1021/jp992325b

3 AUTHORS, INCLUDING:

Howe-Siang Tan
Nanyang Technological University
41 PUBLICATIONS **707** CITATIONS

SEE PROFILE

Role of Pulse Phase and Direction in Two-Dimensional Optical Spectroscopy

Dorine Keusters, Howe-Siang Tan, and Warren S. Warren*

Center for Ultrafast Laser Applications, Department of Chemistry, Princeton University, Princeton, New Jersey 08544

Received: July 12, 1999; In Final Form: September 14, 1999

This paper examines the parallels between magnetic resonance and optical spectroscopy, with the goal of determining to what extent the benefits of 2DNMR might be extended into the optical regime. Precise optical analogues of the simplest 2DNMR sequences (collinear pulse sequences with phased laser pulse generation, phase sensitive detection, and phase cycling) are now feasible, and we demonstrate that they do generate cross-peaks which reveal common energy levels, even when averaged over the distribution of pulse flip angles expected in most optical experiments. One enormous difference between laser and NMR experiments—the use of pulses in different directions in optics—can be exploited to eliminate much of the phase cycling required in NMR. Phase control does permit rotating-frame detection, which is likely to be a substantial practical advantage. Finally, we point out optical analogues of the simplest 2DNMR sequences (COSY and NOESY) will likely add little to our understanding of ultrafast dynamics. Optical analogues of more complex 2D sequences, combining phase control for selective refocusing with noncollinear pulse generation for coherence pathway selection, show more promise.

1. Introduction

Applications of tailored (phase/frequency/amplitude modulated) radio waves are ubiquitous, largely because of technological maturity: generation, propagation, and detection of arbitrary waveforms up to 1 GHz is completely straightforward. The computer and communications revolutions drove these developments, but NMR spectroscopists certainly profited from them decades ago. Coherent spectroscopy—the use of radiation fields with well-defined phase properties to extract information about atoms and molecules—began around 1950 with demonstration of the "spin echo" in nuclear magnetic resonance[1] (a simple two-pulse sequence which separated inhomogeneous from homogeneous line broadening). In the ensuing decades literally hundreds of different NMR pulse sequences (often with shaped radio frequency (rf) pulses) have been developed and are now in routine use by organic chemists to unravel molecular structure. In 1957 Feynman, Vernon, and Hellwarth published a landmark paper pointing out that all two-level systems are mathematically identical[2] and that if coherent light fields were ever created, it would be possible to use these same methods on optical transitions. Not surprisingly, then, the invention of the laser in 1960 was followed quickly by demonstration of the "photon echo"[3]—the optical version of the "spin echo." What is surprising, at least at first glance, is that no comparable expansion of coherent laser pulse sequences has occurred. The vast majority of laser experiments use one or two laser pulses and make the pulses noncollinear or use multiple colors—thus intrinsically averaging the optical phase over a distance comparable to a wavelength. Such sequences (particularly with "ultrafast" laser pulses, which can probe dynamics on a femtosecond time scale) have significantly enhanced our understanding of reaction dynamics and energy transfer.[4] Over the past decade, methods for generating, shaping,[5] and detecting[6] ultrafast laser pulses have been tremendously extended. Ultrafast laser applications are beginning to move more into the scientific mainstream, and optical analogues of many radio frequency applications are just now becoming technologically feasible in a wide range of fields.

To spectroscopists, one of the most tantalizing analogues is "two-dimensional optical spectroscopy": extension of the NMR technique (recognized by Richard Ernst's Nobel Prize) today permits determination of tertiary structure in molecules as large as small proteins. Two-dimensional NMR (2DNMR)[7] permits clean and general detection of coupled spins, either via the through-bond scalar coupling or the through-space nuclear Overhauser effect (NOE). A general method for detecting couplings between chromophores would be particularly valuable in the infrared and could significantly enhance our understanding of energy transport and transient structural changes in chemical reactions.

This paper will examine the parallels between magnetic resonance and optical spectroscopy, with the goal of determining to what extent the benefits of 2DNMR might be extended into the optical regime. We begin with a brief review of the simplest 2DNMR experiments, emphasizing points that are often omitted in textbooks because they are well-understood in the NMR community, but which will turn out to be very important for optical applications. We also review some of the differences between optics and magnetic resonance spectroscopy. We then develop precise optical analogues of the simplest 2DNMR sequences. Our calculations focus on collinear pulse sequences with phased laser pulse generation, phase sensitive detection, and phase cycling. Recent advances in pulse shaping technology make such sequences feasible,[5] and we demonstrate that they do generate cross-peaks which reveal common energy levels, even when averaged over the distribution of pulse flip angles expected in most optical experiments. We then point out that one enormous difference between laser and NMR experiments—the use of pulses in different directions in optics—can be

* To whom correspondence should be addressed. Fax no.: (609) 258-6746. E-mail: wwarren@princeton.edu.

10.1021/jp992325b CCC: $18.00
Published on Web 11/13/1999

exploited to eliminate much of the phase cycling required in NMR. Thus, for example, direct optical implementation of COSY-like (COSY = correlated spectroscopy) sequences with noncollinear pulses turns out not to require explicit phase control over the individual pulses, as has been observed by Hybl and co-workers.[8] Phase control does permit rotating-frame detection,[9] which is likely to be a substantial practical advantage. Finally, we discuss the potential advantages of two-dimensional optical techniques. While optical spectroscopists are usually familiar with only the simplest 2DNMR sequences, we point out that analogues of these sequences will likely add little to our understanding of ultrafast dynamics. Optical analogues of more complex 2D sequences, which combine phase control with noncollinear pulse generation, show more promise.

2. Background: Two-Dimensional NMR

Two-dimensional nuclear magnetic resonance was pioneered in the 1970s with applications of very simple pulse sequences to small molecules.[7] We will briefly review some of the properties of the two best-known early sequences (COSY and NOESY) in order to better understand the possible extensions to optical spectroscopy.

The simplest and best-known two-dimensional pulse sequence is the COSY sequence, which consists of two radio frequency pulses and two delays. Most NMR pulse sequences still use constant-amplitude, constant-frequency ("rectangular") radio frequency pulses for broadband excitation. Rectangular pulses are used not because pulse shaping is difficult (almost all modern NMR spectrometers can generate arbitrary amplitude and frequency modulation)[10] but because it is often unnecessary for the reasons we discuss below. Rectangular pulses are completely specified by their carrier wave frequency, their "flip angle" $\theta = \gamma B_1 t$ (γ is the gyromagnetic ratio, B_1 is the peak field strength, and t is the length) and their phase ϕ with respect to some carrier wave internal to the spectrometer. The most commonly values of θ are 90 and 180°; the most commonly used phases are $\phi =$ (0, 90, 180, 270), which are denoted by subscripts (x, y, $-x$, $-y$), respectively.

In the COSY sequence ($90_x - t_1 - 90_x - t_2$), the entire free induction decay (FID) is sampled for a specific value of t_1, so each application of the pulse sequence leads to signal (heterodyne detected, saving components both in-phase and in-quadrature with respect to the spectrometer's carrier wave) from many different values of the delay t_2. The two channels are then combined into a single complex signal ($I^+ = I_x + iI_y$) which reflects pure absorption. This operator is, of course, non-Hermitian and is only detectable because NMR is an ensemble-averaged experiment. It has recently been recognized that the ability to detect such operators permits some pulse sequence improvements.[11] The sequence is then repeated with different values of t_1, to create a signal array, and processed by complex two-dimensional Fourier transformation.

The calculated two-dimensional spectrum (frequencies f_1 and f_2, respectively) is completely in the "rotating frame" of the carrier wave used to define the phase relation between the two pulses. For example, any signal at $f_2 = 0$ Hz corresponds to exact resonance at the carrier wave frequency, typically hundreds of megahertz.

COSY spectra contain "diagonal peaks" ($f_1 = f_2$) and "antidiagonal peaks" ($f_1 = -f_2$) for all of the resonances. More importantly, they contain "cross-peaks" ($f_1 \neq \pm f_2$) between resonances involving coupled but inequivalent nuclear spins. The nature of the scalar coupling in NMR implies that the cross-peaks reveal which resonances correspond to spins separated by only a few (typically 1−3) chemical bonds.

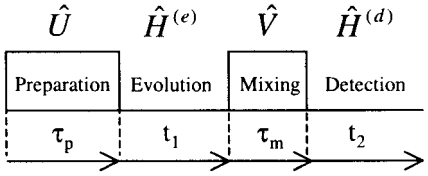

Figure 1. Generic two-dimensional NMR pulse sequence divided into four intervals. The first is a "preparation period" whose pulse sequence generates a propagator $\hat{U}$. The magnetization evolves freely for the evolution period t_1, and then a "mixing period" with propagator $\hat{V}$ is applied. Finally, the magnetization is allowed to evolve freely again for the "detection period" t_2.

Physically close but nonbonded atoms (resulting, for example, from the tertiary structure of a protein) do not give cross-peaks in a COSY experiment but do give cross-peaks in a three pulse experiment ($90_x - t_1 - 90_x - \tau - 90_x - t_2$), called a NOESY experiment. These cross-peaks arise through the nuclear Overhauser effect (hence the acronym) which is essentially the nuclear dipole−dipole interaction averaged over molecular rotation and internal diffusion. The delay τ is typically long (1 s) to let this relaxation mechanism generate a measurable effect.

COSY and NOESY sequences have many desirable features. For example, they are not very sensitive to pulse flip angle errors. In COSY, if the second pulse flip angle is less than 90°, the detected magnetization is reduced and the antidiagonal peaks become weaker than the diagonal peaks. If the first pulse flip angle is less than 90°, some magnetization remains along the z-axis during t_1 and does not evolve during that delay. This reduces the intensity of all the peaks discussed above and creates an additional set of peaks at $f_1 = 0$ Hz. The positions of the cross-peaks (which contain the most important information) are not affected by flip angle errors. The effects of flip angle error in NOESY are similar, but the signal falloff is more rapid as the error increases.

However, it is important to realize that neither COSY nor NOESY extracts molecular information that is inaccessible by other means. Double-resonance selective irradiation experiments (essentially "pump−probe" experiments in optical language) give the same information about which transitions share an energy level.[12] Selective inversion of one resonance, followed by a delay during which the nuclear Overhauser effect perturbs populations of nearby spins, also gives physical proximity.[13] Both of these experiments long predated the development of two-dimensional spectroscopy. COSY and NOESY sequences simply take advantage of what is easy to do in magnetic resonance (apply broadband pulses that completely excite transverse magnetization for all resonances). They substitute N different increments of the indirectly detected delay (and complete detection of the signal, including phase) for N pump−probe experiments with different pump frequencies.

The real power of two-dimensional NMR comes from more complicated sequences, which give information that could not have been obtained by simpler experiments. Historically the first such sequence was very similar to NOESY, except that the second delay was incremented instead of the first ($90_x - \tau - 90_x - t_1 - 90_x - t_2$).[13] If τ is chosen to be at least comparable to the reciprocal of a typical coupling (50−500 ms in isotropic liquids, 1−10 ms in oriented materials), this "multiple-quantum" (MQ) experiment gives resonances from "forbidden" ($\Delta M \neq 1$) transitions in the indirectly detected dimension. It is possible to observe multiple-quantum transitions by continuous irradiation, but the peaks are weak and significantly broadened. In addition, seemingly highly forbidden transitions (such as the

six-spin flip in oriented benzene) can be seen in MQ experiments with transition intensities comparable to the allowed transitions.[13]

In modern NMR texts a generic two-dimensional pulse sequence is divided into four intervals (Figure 1). Starting from an initial density matrix ρ_{init}, we apply a "preparation period" whose pulse sequence generates a propagator $\hat{U}$. The magnetization evolves freely for the evolution period t_1; then a "mixing period" with propagator $\hat{V}$ is applied. Finally, the magnetization is allowed to evolve freely again for the "detection period" t_2. The observed signal can be calculated readily in the Hamiltonian eigenbasis:

$$\begin{aligned}\langle I_x \rangle &= \mathrm{Tr}[I_x \rho(t_1, t_2)] \\ &= \mathrm{Tr}[I_x e^{-i\hat{H}t_2/\hbar}\hat{V}e^{-i\hat{H}t_1/\hbar}\hat{U}\rho_{\text{init}}\hat{U}^{\dagger}e^{i\hat{H}t_1/\hbar}\hat{V}^{\dagger}e^{i\hat{H}t_2/\hbar}] \\ &= \sum_{k,l}(\hat{V}^{\dagger}e^{-i\hat{H}t_2/\hbar}I_x{}^{-i\hat{H}t_2/\hbar})_{kl}\,(\hat{U}\rho_{\text{init}}\hat{U}^{\dagger})_{lk}e^{-i(E_l-E_k)t_1/\hbar} \qquad (1)\end{aligned}$$

with a similar expression for y magnetization. Note that t_1 (the "indirectly detected dimension") only appears in this equation in the final term, which is multiplied by differences in energy between eigenstates. This is the fundamental reason why two-dimensional spectroscopy is useful. Changing $\hat{U}$ and $\hat{V}$ changes the selection rules in the indirectly detected dimension, but the t_1 dependence of the signal accurately reflects how the spins evolved during the evolution period, even though the signal is only detected during t_2. For COSY the preparation and mixing periods contain one pulse each. For NOESY the preparation period is the first pulse, and the mixing period is the last two pulses and intervening delay. For the multiple-quantum sequence the preparation period is the first two pulses and delay, and the mixing period is the final pulse. Note that eq 1 is nonperturbative in nature. The propagators U and V can be (and virtually always are) substantially different from the identity matrix.

Phase cycling also plays an important role in modern pulse sequences. One drawback of the COSY sequence is that the indirectly detected dimension produces two peaks for each resonance, so the spectral bandwidth (hence number of required experiments to achieve a specific final resolution) is twice as large as the normal spectral bandwidth. Mathematically, this arises because the first 90° pulse transforms z-magnetization into y-magnetization, which can be written as a sum of spin raising and lowering operators ($I_y = (I^+ - I_-)/2i$) at positive and negative frequencies, respectively. This problem can be fixed with "hypercomplex detection":[7] repeating the COSY experiment with the first pulse changed to a y pulse. This 90° phase shift in the radio frequency field produces x-magnetization after the second pulse ($I_x = (I_+ + I_-)/2$). Multiplying the signal in the first experiment by i and coadding is then equivalent to saving only the pure raising operator $I_+ = I_x + iI_y$. The antidiagonal peaks are then eliminated, and only half as many values of t_1 are needed. More generally, a transition between two states separated by net absorption of N photons will experience a phase shift of $N\phi$ if all of the pulses used to excite that transition are phase shifted by an amount ϕ. Thus, adding together six multiple-quantum experiments, corresponding to phase shifting the first two pulses by 0, 60, 120, 180, 240, and 300°, would suppress all but the zero- and six-quantum coherences in benzene.[13] In practice it is more common to keep the first two pulse phases constant and instead decrement the phase of the third pulse and the phase of the detecting field, but this is mathematically equivalent.

Over the past few decades, 2DNMR has evolved into an extraordinarily powerful set of techniques for structural determination in molecules as large as small proteins (>25 kDa).[14]

However, none of the sequences above are in common use in their original forms. Modern sequences commonly include irradiation at multiple resonance frequencies (^{1}H, ^{13}C, ^{15}N; 20 pulses are not unusual), gradient pulses to select specific coherence pathways, solvent suppression, and various forms of pulse phase cycling. In general these sequences[14] are optimized to exploit very detailed knowledge about the spin Hamiltonian of a protein.

For example, there are only 20 amino acids; the spectrum of each is well-known and changes little when the amino acid is incorporated into a protein. The scalar coupling between ^{13}C and a directly bonded proton is also nearly independent of spin environment. Thus, it is possible to select a delay to permit complete coherence transfer between these two spins, or even to transfer coherence further along a chain. For these sequences, pulse flip angles and phases are generally critical. Furthermore, the pulse sequences are often designed to alter the effective molecular Hamiltonian during some of the evolution.

The carbon−proton coupling can be averaged away by rotating the carbon magnetization rapidly (compared to the reciprocal of the coupling matrix element).[15] Evolution due to chemical shift differences can be removed with multiple echo pulses.[16] One upper limit of realistic pulse sequence complexity was approached 20 years ago, with "multiple-quantum selective excitation sequences" which actually transferred intensity into selected multiple-quantum coherences rather than simply suppressing the signal from undesired coherences. Sequences with upwards of 1000 pulses were demonstrated experimentally, all with well-defined and important phase relations.[12]

3. Subtle Differences between Laser Spectroscopy and NMR

One important reason why optical multiple-pulse sequences have developed far more slowly than NMR sequences is that implementing useful pulse shaping, phase-controlled multiple pulse sequences, or phase detection with optical fields is technologically much more difficult than in the NMR case. Largely for this reason, programmable pulse shaping with a temporal resolution of 50−100 fs and high powers[17] has played a central role in the recent resurgence of interest in laser selective chemistry and quantum control,[18] and the technological obstacles which seemed formidable for many years have essentially disappeared. There are, however, some fundamental spectroscopic differences which must be seriously considered in evaluating the potential value of optical two-dimensional techniques.

Phrased in the language of optical spectroscopists, all proton NMR transitions have the same dipole moment, all samples are optically thin, NMR transmitters are perfectly stable monochromatic radiation sources, and the entire spectrum has a small bandwidth which means that rectangular pulses easily have a bandwidth which vastly exceeds the entire spectral width. This often makes more complex wave forms unnecesary. None of these assumptions is generally true for laser spectroscopy. These differences are important, but they have been extensively discussed in previous literature.[10,19] Here we will focus on some less obvious effects.

(1) *NMR samples intrinsically absorb and emit circularly polarized radiation.* As soon as the Zeeman interaction of the nuclear dipoles with the external magnetic field exceeds the strength of internuclear dipole−dipole or electric quadrupole

interactions, the *z*-component of the spin angular momentum becomes a good quantum number. Absorption with selection rule $\Delta M = +1$, or emission with selection rule $\Delta M = -1$, then inherently involves the same sense of circularly polarized radiation. The absorbed component depends on the sign of the gyromagnetic ratio, but here for convenience we will assume the right-circularly-polarized (rcp) component is absorbed or emitted. The left-circularly-polarized (lcp) component has essentially no effect in pulsed experiments, although in continuous-wave (cs) experiments it can create a small resonance frequency change known as the Bloch−Siegert shift.[19] Most NMR spectrometers use only a single coil to generate a linearly polarized field, even though this wastes half of the power, because the alternative of arraying two perpendicular coils usually degrades probe performance (although imaging applications, which are often power-limited, sometimes exploit coils which generate circular polarization).

(2) *NMR experiments are virtually always done in the "rotating frame"*. This is a significant advantage, because NMR spectra are narrow: the proton NMR spectrum is typically 10 ppm wide (6 kHz in a 600 MHz spectrometer). Nyquist's theorem then implies that the FID need only be sampled every 166 ms, whereas direct detection of the 600 MHz resonances would normally require nanosecond acquisition time steps. In a multiple-quantum experiment, the benzene six-quantum resonance (at a frequency of 3.6 GHz in a 600 MHz spectrometer) actually appears at only six times the average "resonance offset"[13] (the frequency difference between the carrier wave and the middle of the conventional spectrum). In practice this means t_1 can be incremented in steps of many microseconds, rather than subnanosecond steps.

(3) *Phase shift and pulse delay are completely independent parameters, even for phase modulated pulses which do not have a well-defined carrier wave*. Pulse phase in an NMR spectrometer is usually set by phase shifting the carrier, but, in a more fundamental sense, pulse phase comes primarily from the use of only one component of circularly polarized light for absorption. The concept of a phase shift arises naturally for circularly polarized light, which is readily decomposed into a nonnegative pulse envelope $B_1(t)$ and a phase $\varphi(t)$ without reference to any carrier wave:

$$\vec{B}_1(t) = \hat{x}B_1(t)\cos\varphi(t) + \hat{y}B_1(t)\sin\varphi(t) = \mathrm{Re}[(\hat{x} + i\hat{y})B_1(t)\mathrm{e}^{-i\varphi(t)}] \quad (2)$$

Delaying a pulse by an amount δ is equivalent to replacing $B_1(t)$ with $B_1(t-\delta)$; a phase shift only affects $\varphi(t)$. Nuclear spins can interact with fields in any direction, so the interaction Hamiltonian $\hat{H} = -\vec{\mu}\cdot\vec{B} = -\gamma\vec{I}\cdot\vec{B}$ decomposes into matrix elements along all of the applied field directions. Interaction with a circularly polarized field generates a Hamiltonian with complex matrix elements.

As noted above, most NMR probes generate a linearly polarized field in only one direction. Switching the direction would produce a phase shift; decomposing the field into its lcp and rcp components shows that a phase shift of 90° (switching the magnetic field from $+x$ to $+y$) adds 90° to the rcp component, and subtracts 90° from the lcp component. However, this limitation becomes unimportant because the fractional spectral bandwidth is small, so, for useful pulse sequences, the time dependence of the phase becomes much slower if we assume a carrier frequency ω:

$$\varphi(t) = -\omega t + \phi(t)$$
$$\vec{B}_1(t) = \hat{x}B_1(t)\cos(\omega t - \phi(t)) = \mathrm{Re}[(\hat{x} + i\hat{y})B_1(t)\,\mathrm{e}^{-i(\omega t - \phi(t))}] + \mathrm{lcp} \quad (3)$$

Now a phase shift corresponds to a delay in the maximum of the carrier wave without changing the envelope $B_1(t)$. As long as $B_1(t)$ varies little in time $1/\omega$ (the slowly varying envelope approximation), the lcp wave has no significant Fourier component at the resonance frequency and can be ignored. In translating to the rotating frame, the phase shift $\phi(t)$ becomes an apparent change in direction of the field. There is no requirement that $B_1(t)$ encompass an exactly integral number of cycles of the carrier frequency, so changing the phase can change the area (in the laboratory frame) but does not change $B_1(t)$ when the slowly varying envelope approximation is valid.

(4) *Nuclear induction does not generate electromagnetic waves.* Sample dimensions are virtually always much smaller than a wavelength, so detection takes place in what would be called the near-field limit in optics. The spins do not generate an electric field perpendicular to their magnetic field. It would be technically possible to apply radio frequency pulses with magnetic fields pointed in different directions, but the only effect of the direction change would be to give an apparent phase shift, which is done more simply in the rotating frame.

(5) *The NMR high-temperature limit imposes additional selection rules in the simplest pulsed experiments.* For the dynamics of a two-level system the temperature appears only as a scale factor which reduces the macroscopic magnetization. It has more significant consequences for multilevel systems. N coupled spins give $2N$ energy levels, but the energy difference between the highest and lowest spin states is still virtually always much less than kT in solution, so even the highest states are heavily populated. This is the fundamental reason why a multiple-quantum NMR experiment requires three pulses. Single-pulse excitation from the high-temperature equilibrium density matrix produces only single-spin operators, and couplings need to act during two separate time periods (during the delay τ to create multispin operators and during the delay t_2 to make them detectable). There is one recent significant exception to these statements: dipolar couplings between distant spins in solution permit detection of intermolecular multiple-quantum coherences in two-pulse experiments if the solution is concentrated.[20]

In ultrafast laser spectroscopy, the situation is somewhat different:

(1) *Linearly polarized fields are more common than circularly polarized fields, because molecular transition dipole moments are anisotropic.* Most lasers produce linearly polarized light at their output, and circularly polarized fields are notoriously difficult to propagate (reflection off mirrors often produces elliptical polarization).[21] In addition, nuclear spins can interact with a magnetic field in any direction, but the transition electric dipole moment for nondegenerate states has a well-defined vector orientation in the molecular frame. Thus the excitation process is simpler to visualize with linearly polarized light.

(2) *Optical experiments are virtually never done in the "rotating frame", even when the fractional bandwidth is small.* Photodiodes and photomultipliers detect intensity only. Heterodyne detection is more difficult and requires a reference wave, which is phase-coherent with the laser pulses.

(3) *Phase shifting is a much more subtle concept for linearly polarized transitions. The most common method of pulse sequence design couples delays and phase shifts*. Phase shifts

again are easy to define unambiguously with circularly polarized light, which can be decomposed into a nonnegative pulse envelope $\epsilon(t)$ and a phase $\varphi(t)$ without reference to any carrier wave:

$$\vec{\epsilon}_1(t) = \hat{x}\epsilon_1(t)\cos\varphi(t) + \hat{y}\epsilon_1(t)\sin\varphi(t) = \mathrm{Re}[(\hat{x} + i\hat{y})\epsilon_1(t)\, e^{-i\varphi(t)}] \quad (4)$$

The phase difference between any two waves (at a specified position and time) is unambiguous whenever neither field vanishes; it is merely the angle between the electric field vectors.

Delaying a pulse by an amount δ is equivalent to replacing $\epsilon_1(t)$ with $\epsilon_1(t-\delta)$; a phase shift only affects $\varphi(t)$. Again switching the direction would produce a phase shift with opposite signs for the rcp and lcp components. When circularly polarized light can induce circular molecular polarization (for example, in optical transitions involving p electrons), the optical and NMR pictures of phase are quite similar. Unfortunately, in the more common linear dipole case, setting up the optical analogue of an NMR two-level system requires orienting the transition electric dipole in the *xy*-plane (say along the *x*-direction). Changing the electric field direction fundamentally changes the physical interaction; a *y*-polarized electric field would cause no absorption. Interaction with a circularly polarized field generates an interaction Hamiltonian with only real matrix elements, as opposed to the NMR case. For linearly polarized light along the *x*-direction,

$$\vec{\epsilon}_1(t) = \hat{x}\epsilon_1(t)\cos\varphi(t) = {}^1/_2\mathrm{Re}[(\hat{x} + i\hat{y})\epsilon_1(t)(e^{-i\varphi(t)} + e^{i\varphi(t)})] \quad (5)$$

Hence there is an intrinsic phase ambiguity, since positive and negative shifts cannot be distinguished experimentally. Phase becomes a useful concept again only if we can introduce a carrier wave. Instead of decomposing the interaction into rcp and lcp components, as in the NMR case, we decompose the interaction Hamiltonian into "rotating" and "counterrotating" components

$$\begin{aligned} \varphi(t) &= -\omega t + \phi(t) \\ H &= -\vec{\mu}\cdot\vec{\epsilon}_1(t) \\ &= d_1(t)\cos(\omega t - \phi(t)) \\ &= {}^1/_2 d_1(t)(e^{-i(\omega t-\phi(t))} + e^{i(\omega t-\phi(t))}) \end{aligned} \quad (6)$$

Now a phase shift corresponds to a delay in the maximum of the carrier wave without changing the envelope $d_1(t)$; a time delay of δ corresponds to replacing $d_1(t)$ with $d_1(t-\delta)$. The difference between a phase shift of $+\phi$ and a phase shift of $-\phi$ physically translates into lagging or leading the carrier wave, as long as $\phi(t)$ and $d_1(t)$ vary little in time $1/\omega$ (the slowly varying envelope approximation). In that case the counterrotating wave has no significant Fourier component at the resonance frequency and can be ignored.

Jonas and co-workers have also recently considered the issue of phase shift versus pulse delay for linearly polarized light[9] from a rather different perspective. They distinguish between phase shifts in the time domain and phase shifts in the frequency domain. They define a phase shift in the frequency domain (essentially what we call φ here) by Fourier transforming the optical field, multiplying positive frequency components by $e^{i\varphi}$, multiplying negative frequency components by $e^{-i\varphi}$, and noting an ambiguity at $\omega = 0$. The complexity is inherent in the use of linearly polarized light, and the ambiguity at $\omega = 0$ is easily understood from the arguments above. They thus distinguish a phase shift from a time delay, which corresponds to a linear phase shift with frequency. The difficulty with this definition is that pulses with a small fractional bandwidth always have rapidly varying $\varphi(t)$; hence, we will use $\phi(t)$ as the phase in this work.

Modern ultrafast laser systems work with a pulse repetition rate far slower than molecular dynamics; for amplified pulses, one pulse per millisecond (1 kHz) is typical. Pulse sequences are created by splitting the pulse from the laser system and then sending multiple copies along different paths. Changing a path length delays both the envelope and the effective carrier; thus, a delay will inherently create a phase shift.

A variety of methods have been introduced to control phase and delay independently. For example, a CW laser beam can be modulated by a radio frequency pulse sequence in an acoustooptic modulator (AOM),[22] in a way directly analogous to NMR pulse sequence generation, but this gives nanosecond rise times and low peak powers with existing modulators and lasers. The most common femtosecond pulse shaping methods spatially disperse the spectrum to independently modulate the different frequency components.[5] If the spatial modulator is an acoustooptic modulator, shifting the rf driving frequency corresponds to generating a delay; phase shifting the rf would phase shift the laser pulse.[23]

(4) *Most optical experiments do generate electromagnetic waves.* Optical experiments are usually done with chromophores distributed in a sample volume much larger than λ^3 and usually use electromagnetic waves that propagate from a distant source. Changing the direction of propagation introduces a position-dependent phase shift. Two sine waves with the same frequency ω but different directions $\mathbf{k}$ and $\mathbf{k} + \Delta\mathbf{k}$ will constructively and destructively interfere at different positions and assume all possible phases over a distance $2\pi/|\Delta\mathbf{k}|$ in the direction of the wave vector difference. Optical spectroscopists have long used this to advantage in simple experiments, such as the photon echo,[24] to separate weak signals from strong laser pulses by direction. As we discuss in the last section (consistent with recent experimental results by Hybl and co-workers[8]), this directional variation can also be used to eliminate much of the phase cycling needed in NMR experiments. However, for experiments with samples much smaller than λ^3, such as single ion spectroscopy,[25] the seperation of signal by directional detection does not apply, and phase-cycling schemes may still be useful.

(5) *Optical transitions often leave the low-temperature limit.* This means that a single pulse can induce multiphoton transitions from the ground state, as opposed to the NMR case. However, there is an important subtlety. If the energy level diagram is unbounded and accessible via allowed transitions within the pulse bandwidth, 90 and 180° pulses may be impossible. The energy levels in a perfect harmonic oscillator, for example, can only be excited into a coherent state. Thus, anharmonicity plays a critical role unless only very small excitations are desired.

4. Direct Optical Analogues of Two-Dimensional NMR

In this section we will describe experimentally feasible two-dimensional optical experiments which are the direct mathematical analogue of the NMR COSY experiment. These experiments have the following properties:

(1) All pulses are assumed to be collinear, with well-defined interpulse phase relations. Albrecht and co-workers define this as carrier-delayed pulses.[9]

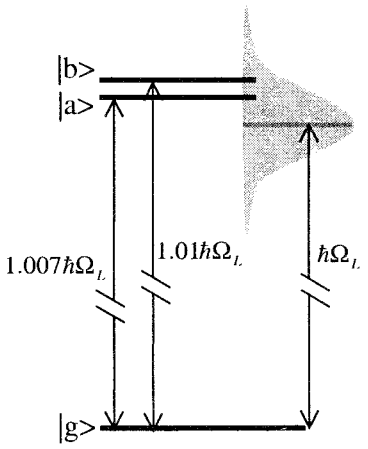

Figure 2. Energy level diagram of the three level system used in section 4.1. The detuning frequencies are $\omega_{ag} = 0.007\Omega_L$ and $\omega_{bg} = 0.01\Omega_L$, where Ω_L is the laser center frequency.

(2) Phase-sensitive detection in the rotating frame is achieved by adding one more pulse and detecting the excited-state population when the pulse is phase-cycled. The final pulse serves the same purpose as the time-gated heterodyne detection that uses phase-locked pulses to separate the real and imaginary part of the nonlinear response function in stimulated photon echo experiments. This method, first demonstrated by Warren and Zewail for nanosecond pulses,[26] was later extended to picosecond[27] and subpicosecond[28] and exploits the rotational properties of the pseudopolarization vector. The rotating-frame x component of the pseudopolarization vector is converted into $-z$ by a pulse with phase y, or into $+z$ by a pulse with phase $-y$. The difference between these two states is a difference in the excited-state population. Similarly, the y component of the pseudopolarization vector can be detected by x and $-x$ pulses.

Converting the polarization to detectable excited-state population with an additional pulse is not quite the same as obtaining the real and imaginary part of the polarization by heterodyne detection with a reference field that does not pass through the sample: the equivalence of these experiments clearly requires an optically thin sample. Jonas has recently noted[9] an interesting additional difference: the observed signal with phase-locked pulses is not affected by the dispersive part of the susceptibility (in the small flip angle limit) if all pulses pass through sample. For example, each pulse would experience the same phase shift due to propagation through media with an index of refraction unequal to 1.

(3) In an NMR COSY experiment, one never observes multiple-quantum (multiphoton) transitions in the indirectly detected dimension as discussed above. In an optical COSY experiment, multiphoton transitions will occur unless the pulse flip angles are very small. These transitions can be selected by phase shifting the first pulse.

4.1. Theory. Consider a three-level model system (Figure 2) where the ground state is coupled by the laser to both excited states a and b.

The Hamiltonian for interaction of light with matter in the semiclassical approximation can be written as

$$\hat{H}(t) = \hat{H}_0 - \hat{\mu}\cdot\vec{E}(t) \tag{7}$$

Where $\hat{H}_0$ is the time-independent molecular Hamiltonian $\sum_i E_i|i\rangle\langle i|$ in the absence of the field. $\hat{\mu}$ is the transition dipole moment operator

$$\hat{\mu} = \vec{\mu}_{eg}|e\rangle\langle g| + \vec{\mu}_{ge}|g\rangle\langle e| \tag{8}$$

$|e\rangle$ can represent either $|a\rangle$ or $|b\rangle$. The classical electric field $\vec{E}(t)$ in eq 7 is described as

$$\vec{E}(t) = \vec{A}(t)\, e^{-i(\Omega_L t-\phi)} + cc \tag{9}$$

where $\vec{A}(t)$ is the (real) amplitude of the pulse envelope, ϕ is the phase of the pulse, and Ω_L is the laser center frequency.

The Hamiltonian for the three level system described in Figure 2 can be repartitioned to become (cast in the matrix form)

$$\hat{H} \equiv \hat{H}_{rot.} + \hat{H}' = \begin{pmatrix} 0 & 0 & 0 \\ 0 & \hbar\Omega_L & 0 \\ 0 & 0 & \hbar\Omega_L \end{pmatrix} + \begin{pmatrix} 0 & V\cos(\Omega_L t-\phi) & V\cos(\Omega_L t-\phi) \\ V\cos(\Omega_L t-\phi) & E_a - \hbar\Omega_L & 0 \\ V\cos(\Omega_L t-\phi) & 0 & E_b - \hbar\Omega_L \end{pmatrix} \tag{10}$$

where we have referenced the ground-state energy to be zero and $V(t) = -\vec{\mu}_{ge}\cdot\vec{A}(t)/2$. The partitioning allows the time-dependent Schrödinger equation to be cast in the interaction picture

$$i\hbar\frac{\partial\psi_{int}}{\partial t} = \hat{H}_{int}\psi_{int} \tag{11}$$

where we have

$$\hat{H}_{int} = e^{i\hat{H}_{rot.}t/\hbar}\hat{H}'e^{-i\hat{H}_{rot.}t/\hbar} = \begin{pmatrix} 0 & Ve^{i\phi} & Ve^{i\phi} \\ Ve^{-i\phi} & \hbar\omega_a & 0 \\ Ve^{-i\phi} & 0 & \hbar\omega_b \end{pmatrix} \tag{12}$$

where $\omega_{a,b} = E_{a,b}/\hbar - \Omega_L$. Note also that the rotating wave approximation has been evoked. The procedure outlined effectively discards terms oscillating at optical frequencies. This is entirely analogous to the intuitive Bloch vector for a two level system in a rotating frame[19] and can be expanded to include any arbitrary number of states.

If we further assume that the laser pulses used have a square shape in the time domain, then the density matrix of the system after a series of pulses and delays can be solved by a series of propagation operators with time-independent Hamiltonians. For instance, the density matrix after three square pulses of similar constant real amplitude $A(t) = A_0$ and phase of ϕ_1, ϕ_2, and ϕ_3 with delays t_1 and t_2 between them can be written as

$$\rho(t_1, t_2) = e^{-i\hat{H}_{on}\tau}\, e^{-i\hat{H}_{off}t_1}\, e^{-i\hat{H}_{on}\tau}\, e^{-i\hat{H}_{off}t_2}\, e^{-i\hat{H}_{on}\tau} \times \rho_{init} e^{i\hat{H}_{on}\tau}\, e^{i\hat{H}_{off}t_2}\, e^{i\hat{H}_{on}\tau}\, e^{i\hat{H}_{off}t_1}\, e^{i\hat{H}_{on}\tau} \tag{13}$$

where $\hat{H}_{on}$ is the interaction Hamiltonian when the laser pulse is on for the duration of the pulse length τ (eq 12) and $\hat{H}_{off}$ is the interaction Hamiltonian when the laser pulse is off (i.e. with $V = 0$ in eq 12).

In this experiment, the total fluorescence emitted after the third pulse is measured as a function of delays t_1 and t_2. This will be proportional to the populations in the excited states and hence proportional to the sum of the two diagonal elements $\rho_{aa}(t_1, t_2) + \rho_{bb}(t_1, t_2)$ of the density matrix in eq 13. A two-dimensional Fourier transform of this signal, which oscillates with the detuning frequency or difference frequency between

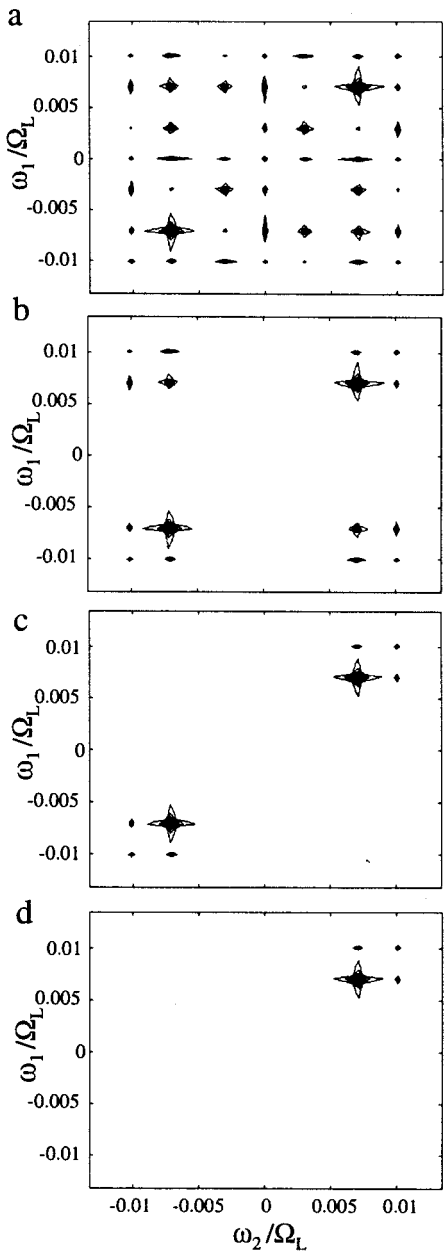

Figure 3. Two-dimensional spectra of the three level system described in Figure 2. (The unit for both axes is Ω_L, the center laser frequency): (a) spectrum without any phase cycling; (b) spectrum of the four cycle experiment described in eq 16; (c) spectrum of the eight cycle experiment described in eq 21; (d) spectrum with the sixteen cycle experiment described in eq 22.

transitions, yields the two-dimensional spectrum. For an experiment in which all three pulses have the same phase, the spectrum is given in Figure 3a. The scale of the axes is the ratio of the resulting frequencies to the center laser frequency. ω_a and ω_b were chosen to be $0.007\Omega_L$ and $0.01\Omega_L$, respectively. The pulse area ($V\tau/2$) is chosen to be 0.4π, and the length of a pulse is 100 fs.

It can be seen that apart from the frequency components ω_a and ω_b many other frequency components are present, at $\omega_{1,2} = 0$; $\omega_{1,2} = \pm(\omega_a - \omega_b)$; $\omega_{1,2} = \pm\omega_a$ and $\omega_{1,2} = \pm\omega_b$.

These spurious frequency components do not contain any additional information, but they can be very strong, making interpretation of the spectra more difficult.

The full expression of $\rho_{aa} + \rho_{bb}$ contains 36 terms, each containing a different oscillation frequency during t_1 and t_2

TABLE 1: The 36 Terms for the Expression $\rho_{aa} + \rho_{bb}$ for the Three Level System Summarized in Equation 14.[a]

i	ω_1	ω_2	ϕ_1	ϕ_2	ϕ_3
1	0	0	1	1	1
2	$\pm(\omega_b - \omega_a)$	0	1	1	1
3	0	$\pm(\omega_b - \omega_a)$	1	1	1
4	$\pm(\omega_b - \omega_a)$	$\pm(\omega_b - \omega_a)$	1	1	1
5	$-\omega_a$	0	$e^{-i\phi_1}$	$e^{i\phi_2}$	1
6	ω_a	0	$e^{i\phi_1}$	$e^{-i\phi_2}$	1
7	$-\omega_b$	0	$e^{-i\phi_1}$	$e^{i\phi_2}$	1
8	ω_b	0	$e^{i\phi_1}$	$e^{-i\phi_2}$	1
9	0	$-\omega_a$	1	$e^{-i\phi_2}$	$e^{i\phi_3}$
10	0	ω_a	1	$e^{i\phi_2}$	$e^{-i\phi_1}$
11	0	$-\omega_b$	1	$e^{-i\phi_2}$	$e^{-i\phi_3}$
12	0	ω_b	1	$e^{-i\phi_2}$	$e^{-i\phi_3}$
13	$\pm(\omega_b - \omega_a)$	$-\omega_a$	1	$e^{-i\phi_2}$	$e^{i\phi_3}$
14	$\pm(\omega_b - \omega_a)$	ω_a	1	$e^{i\phi_2}$	$e^{-i\phi_3}$
15	$\pm(\omega_b - \omega_a)$	$-\omega_b$	1	$e^{-i\phi_2}$	$e^{i\phi_3}$
16	$\pm(\omega_b - \omega_a)$	ω_b	1	$e^{i\phi_2}$	$e^{-i\phi_3}$
17	$-\omega_a$	$\pm(\omega_b - \omega_a)$	$e^{-i\phi_1}$	$e^{i\phi_2}$	1
18	ω_a	$\pm(\omega_b - \omega_a)$	$e^{i\phi_1}$	$e^{-i\phi_2}$	1
19	$-\omega_b$	$\pm(\omega_b - \omega_a)$	$e^{-i\phi_1}$	$e^{i\phi_2}$	1
20	ω_b	$\pm(\omega_b - \omega_a)$	$e^{i\phi_1}$	$e^{-i\phi_2}$	1
21	ω_a	$-\omega_a$	$e^{i\phi_1}$	$e^{-i2\phi_2}$	$e^{i\phi_3}$
22	ω_b	$-\omega_a$	$e^{i\phi_1}$	$e^{-i2\phi_2}$	$e^{i\phi_3}$
23	ω_a	$-\omega_b$	$e^{i\phi_1}$	$e^{-i2\phi_2}$	$e^{i\phi_3}$
24	ω_b	$-\omega_b$	$e^{i\phi_1}$	$e^{-i2\phi_2}$	$e^{i\phi_3}$
25	$-\omega_a$	ω_a	$e^{-i\phi_1}$	$e^{i2\phi_2}$	$e^{-i\phi_3}$
26	$-\omega_b$	ω_a	$e^{-i\phi_1}$	$e^{i2\phi_2}$	$e^{-i\phi_3}$
27	$-\omega_a$	ω_b	$e^{-i\phi_1}$	$e^{i2\phi_2}$	$e^{-i\phi_3}$
28	$-\omega_b$	ω_b	$e^{-i\phi_1}$	$e^{-i2\phi_2}$	$e^{-i\phi_3}$
29	$-\omega_a$	$-\omega_a$	$e^{-i\phi_1}$	1	$e^{i\phi_3}$
30	$-\omega_b$	$-\omega_a$	$e^{-i\phi_1}$	1	$e^{i\phi_3}$
31	$-\omega_a$	$-\omega_b$	$e^{-i\phi_1}$	1	$e^{i\phi_3}$
32	$-\omega_b$	$-\omega_b$	$e^{-i\phi_1}$	1	$e^{i\phi_3}$
33	ω_a	ω_a	$e^{i\phi_1}$	1	$e^{-i\phi_3}$
34	ω_b	ω_a	$e^{i\phi_1}$	1	$e^{-i\phi_3}$
35	ω_a	ω_b	$e^{i\phi_1}$	1	$e^{-i\phi_3}$
36	ω_b	ω_b	$e^{i\phi_1}$	1	$e^{-i\phi_3}$

[a] Only rows 33−36 are selected by the phase cycling sequence described by eq 22.

(corresponding to different peaks on the 2-D spectra), with their coefficients dependent on the phases of the three pulses ϕ_1, ϕ_2, and ϕ_3

$$\rho_{aa} + \rho_{bb} = \sum_{i=1}^{36} a_i(V)\, c_i(\phi_1, \phi 2, \phi 3) e^{i\omega_1 t_1} e^{i\omega_2 t_2} \qquad (14)$$

The expression for $c_i(\phi_1, \phi_2, \phi_3)$'s for various ($\omega_1$, ω_2) are given in Table 1. The components in rows 33−36 of Table 1 suffice to tell us the information that we seek.

The intensity of the signal for a particular frequency pair, for example ($\omega_1 = 0$, $\omega_2 = -\omega_a$), can be written as

$$I_{0,-\omega_a} = I'_{0,-\omega_a}(1) e^{-i\phi_2} e^{i\phi_3} \qquad (15)$$

From Table 1 it can be seen that the part of the signal that oscillates with the difference frequency $\pm(\omega_a - \omega_b)$ or that is constant during the second propagation time t_2 (rows 1−8 of Table 1) does not depend on the phase of the third pulse. Therefore a two-experiment phase cycle, consisting of the subtraction of two experiments with phase of $\phi_3 = \pi$ in the last pulse (written as $XXX - XX\bar{X}$), will eliminate these components. Similarly, cycling the phase of the second pulse: $XXX - X\bar{X}X$ will eliminate the same components during the first propagation time (rows 9−16 of Table 1). Hence, the elimination of the components from rows 1−16 can only be achieved by conducting a four-experiment cycle

$$XXX - XX\bar{X} + X\bar{X}X - X\bar{X}\bar{X} \quad (16)$$

This can be illustrated by considering the example of the component with 0, $-\omega_a$. After phase cycling this becomes

$$I_{0,-\omega_a} = I'_{0,-\omega_a}[(1)(1)(1)-(1)(1)(-1) + (1)(-1)(1) - (1)(-1)(-1)] = 0 \quad (17)$$

The spectrum after such a four-cycle experiment is given in Figure 3b. Peaks at $\omega_1 = \pm\omega_{a,b}$ and $\omega_2 = \pm\omega_{a,b}$ will not be eliminated. Phase-cycling schemes that will achieve the same are

$$XYX - XY\bar{X} + X\bar{Y}X - X\bar{Y}\bar{X} \quad (18)$$

$$XYY - XY\bar{Y} + X\bar{Y}Y - X\bar{Y}\bar{Y} \quad (19)$$

$$XXY - XX\bar{Y} + X\bar{X}Y - X\bar{X}\bar{Y} \quad (20)$$

Y and $\bar{Y}$ being pulses with phase $\phi = \pi/2$ and $\phi = -\pi/2$; respectively. An eight-sequence cycle such as

$$XXX - XX\bar{X} + X\bar{X}X - X\bar{X}\bar{X} + XYX - XY\bar{X} + X\bar{Y}X - X\bar{Y}\bar{X} \quad (21)$$

will eliminate signals with components ($\pm\omega_{a,b}$, $\mp\omega_{a,b}$) and ($\pm\omega_{a,b}$, $\mp\omega_{b,a}$). (Terms 21−28 of Table 1) but not the signals ($\omega_{a,b}$, $\omega_{a,b}$) and ($-\omega_{a,b}$, $-\omega_{a,b}$) (Figure 3c) (In all spectra plotted in this paper, the strongest peak has been scaled to 1, ignoring the DC component.)

Finally, the terms with ($-\omega_{a,b}$, $-\omega_{a,b}$) and ($-\omega_{b,a}$, $-\omega_{a,b}$) can be eliminated by doing a 16-cycle experiment:

$$XXX - XX\bar{X} + X\bar{X}X - X\bar{X}\bar{X} + XYX - XY\bar{X} + X\bar{Y}X - X\bar{Y}\bar{X} + i[XYY - XY\bar{Y} + X\bar{Y}Y - X\bar{Y}\bar{Y} + XXY - XX\bar{Y} + X\bar{X}Y - X\bar{X}\bar{Y}] \quad (22)$$

This 16-cycle will give a spectrum with the minimum number of peaks, simplifying the interpretation of the spectrum (Figure 3d).

4.2. Examples. *4.2.1. Seven Level System.* The calculations described in the previous paragraph were extended to two multilevel systems with different types of coupling. The rotating picture energy diagram of a seven level system is illustrated in Figure 4, while the corresponding hamiltonian is as shown in Chart 1. In this case two levels such as e_1 and e_2 are coupled through two transitions involving their common ground-state g_1. All transition dipole moments are chosen to be the same at 1 D. Different transition dipole moments will vary the intensity of the various peaks, but it will not influence the position of the peaks, nor will it affect the effect of the phase-cycling scheme. These spectra are averaged over a Gaussian intensity distribution to simulate a TEM_{00} mode of a Gaussian beam with a maximum pulse area of 2π at the spatial center of the pulse. Compare the non-phase-cycled spectra in Figure 5a with the 16-cycle spectrum plotted in Figure 5b. Even for a relatively small system such as this, interpretation of Figure 5a would be difficult. However, the peaks in the phase-cycled spectrum in Figure 5b can be readily interpreted. Peak numbers 1−5 correspond to transitions 1−5, as indicated in Figure 4. Peaks 6 correspond to the cross-terms between transitions e_1-g_1 and e_2-g_1, since they are coupled through their common ground state. Similarly, peaks 7 are the cross-peaks between transitions e_1-g_1 and e_3-g_1 and peaks 8 the cross-peaks between transitions e_2-g_1 and e_3-g_1. Finally, peaks 9 are the cross-terms between transitions e_4-g_2 and e_5-g_2. Note the absence of cross-peaks between for example transition e_1-g_1 and e_4-g_2, since there is no coupling between levels e_1 and e_4. The small peaks between the diagonal peaks 2 and 4 and peaks 3 and 5 are caused by the overlap of the tails of these peaks and are not caused by any physical couplings. It has been verified that by increasing the resolution, these peaks will disappear.

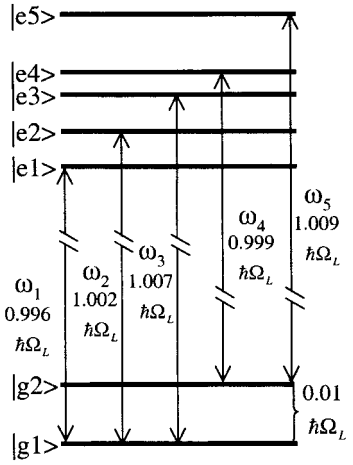

Figure 4. Energy level diagram of the seven level system used in this simulation in section 4.2.1. In equation 23 the corresponding Hamiltonian is given in the rotating picture with $V = -1/2A\mu$. A is the amplitude of the square laser pulse envelope and μ is the effective transition dipole moments (set at 1 D in this simulation).

4.2.2. Four Level System: Two Coupled Chromophores. The model system used in this example consists of two coupled chromophores and is illustrated in Figure 6. As suggested by Zhang and co-workers,[29] such a model can be applied to a wide range of interesting physical systems. These include molecular aggregates[30] and amide-I bands in proteins.[31] The knowledge of the strength of the couplings between chromophores can often provide structural information for these systems. In this simulation, the two chromophores have transition energies of $E_a = 1.008\hbar\Omega_L$ and $E_b = 0.996\hbar\Omega_L$, where Ω_L is the center frequency of the laser pulse used. The double-exciton state will hence be at $2.004\hbar\Omega_L$. The transition dipole moments are set at 0.02 and 0.018 D, respectively. A pulse length of 200 fs and peak electric field strength of 8.0×10^9 V/m is used. This corresponds to an area of $\approx$1.0 rads.

The Hamiltonian for the two coupled chromophores system

CHART 1

$$\hat{H}_{local} = \begin{pmatrix} \hbar\omega_{g1} & 0 & V_1(t) & V_2(t) & V_3(t) & 0 & 0 \\ 0 & \hbar\omega_{g2} & 0 & 0 & 0 & V_4(t) & V_5(t) \\ V_1(t) & 0 & \hbar(\omega_{e1}-\Omega_L) & 0 & 0 & 0 & 0 \\ V_2(t) & 0 & 0 & \hbar(\omega_{e2}-\Omega_L) & 0 & 0 & 0 \\ V_3(t) & 0 & 0 & 0 & \hbar(\omega_{e3}-\Omega_L) & 0 & 0 \\ 0 & V_4(t) & 0 & 0 & 0 & \hbar(\omega_{e4}-\Omega_L) & 0 \\ 0 & V_5(t) & 0 & 0 & 0 & 0 & \hbar(\omega_{e5}-\Omega_L) \end{pmatrix} \quad (23)$$

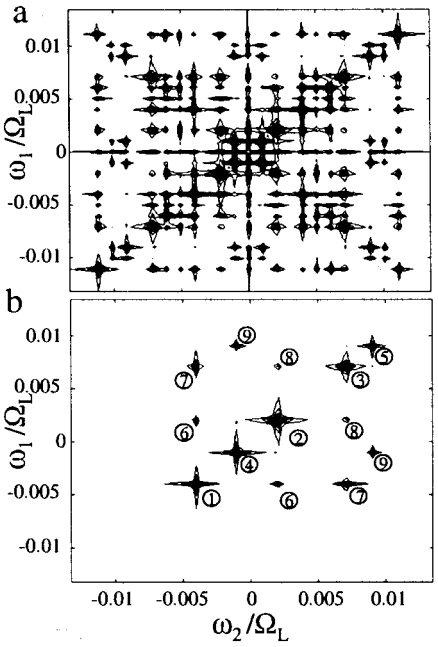

Figure 5. Two-dimensional spectra of the seven level system described in Figure 4 (the unit for both axes is Ω_L, the center laser frequency): (a) spectrum without any phase cycling; (b) spectrum with the sixteen cycle experiment described in eq 22. Peaks 1−5 correspond to transitions 1−5 as indicated in Figure 4. Peak 6 corresponds to the cross-terms between coherences e_1-g_1 and e_2-g_1. Peak 7 is the cross-peak between coherences e_1-g_1 and e_3-g_1 and peak 8 the cross-peak between coherences e_2-g_1 and e_3-g_1. Peak 9 is the cross-term between coherences e_4-g_2 and e_5-g_2.

expressed in the local excitation basis set is

$$\hat{H}_{\text{local}} = \begin{pmatrix} 0 & 0 & 0 & 0 \\ 0 & E_a & \kappa & 0 \\ 0 & \kappa & E_b & 0 \\ 0 & 0 & 0 & E_a + E_b \end{pmatrix} \tag{24}$$

where κ defines the strength of the coupling. This Hamiltonian can be diagonalized and expressed in the coupled basis set. After introducing the coupling with the radiation field, the Hamiltonian in the coupled basis set can be repartitioned as

$$\hat{H}_{\text{coupled}} \equiv \hat{H}_{\text{rot.}} + \text{H}'$$

$$= \begin{pmatrix} 0 & 0 & 0 & 0 \\ 0 & \hbar\Omega_L & 0 & 0 \\ 0 & 0 & \hbar\Omega_L & 0 \\ 0 & 0 & 0 & 2\hbar\Omega_L \end{pmatrix} + \begin{pmatrix} 0 & V_1(t) & V_2(t) & 0 \\ V_1(t) & E_+ - \hbar\Omega_L & 0 & V_3(t) \\ V_2(t) & 0 & E_- - \hbar\Omega_L & V_4(t) \\ 0 & V_3(t) & V_4(t) & E_+ + E_- - 2\hbar\Omega_L \end{pmatrix} \tag{25}$$

where $V_n(t)$ is the coupling with the optical field in the coupled basis, $V_n(t) = V_n \cos(\Omega_L t - \phi)$ and $E_\pm = {}^1/_2(E_a + E_b \pm [(E_a - E_b)^2 + 4|\kappa|^2]^{1/2})$. The time-independent interaction picture Hamiltonian, analogous to eq 12 can then be obtained.

The two-dimensional spectra with full phase cycling were calculated for different values of coupling κ. For $\kappa = 0$, whereby the two chromophores are decoupled, the 2-D spectrum is shown in Figure 7a. The two peaks correspond to the detuning frequencies of the chromophores. For a coupling of $\kappa = 0.005\hbar\Omega_L$, the 2-D spectrum is shown in Figure 7b, the cross-peaks arise from the coupling between the two chromophores. The intensity of the cross-peaks reflects the strength of the coupling.

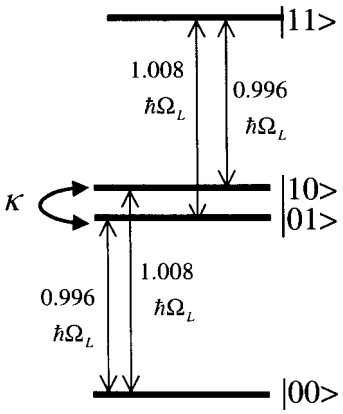

Figure 6. Energy level diagram for two chromophores coupled through interaction κ. The states are in the local excitation basis. The Hamiltonian describing the system is given in eq 24.

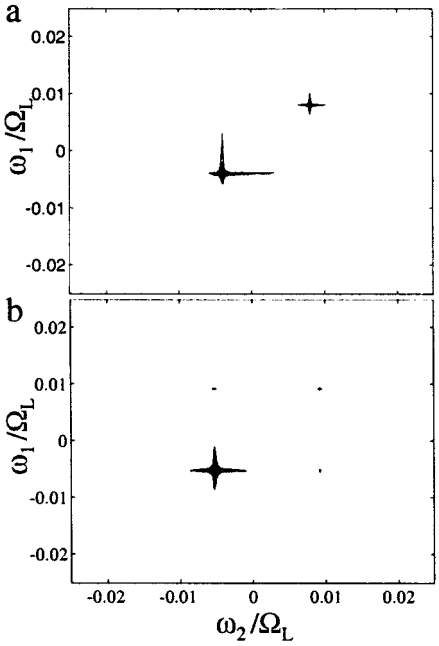

Figure 7. Two-dimensional spectra of two coupled chromophores described in Figure 6 (The unit of both axes is Ω_L, the laser center frequency): (a) spectrum when system has no coupling, $\kappa = 0$; (b) spectrum when system has a coupling of $\kappa = 0.005\hbar\Omega_L$.

4.3. Comparison: Directional Detection vs Phase Cycling. By using the approximation of square pulses and evoking the rotating frame picture, we can use a time-independent Hamiltonian during each pulse and thus explicitly write out eq 1 in terms of rotation operators. Such a treatment is the exact mathematical analogue of a COSY experiment, with one exception. In a COSY experiment, restriction to the high-temperature limit implies that only single-photon transitions have been excited at the beginning of t_1; in the optical experiment, multiphoton transitions can be excited as well.

For the purposes of comparison between optical and NMR methods, we will instead use the standard optical technique of expanding the propagation operator in a perturbative series. Such an expansion only makes sense if the propagators $\hat{U}$ and $\hat{V}$ in eq 1 in fact do not grossly perturb the population, but this is the usual limit with ultrafast laser pulses (which rarely have

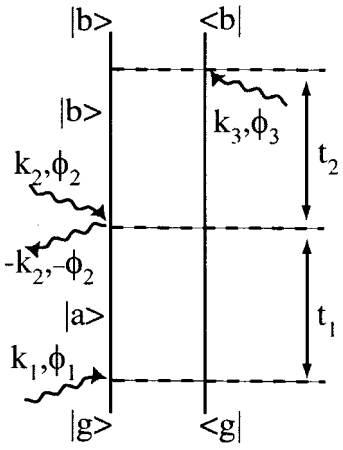

Figure 8. One of the double-sided Feynman diagrams representing the coherence transfer pathway that gives the desired two-dimensional spectrum. It is the visual representation of eq 27. Each interaction is labeled by the phase and **k**-vector of the optical pulse. By using the phase cycling scheme described in eq 22, only the pathway represented by this diagram shows up in the spectrum.

significant flip angle). We take this approach to show that, in fact, the procedure of phase cycling is very much analogous to the direction-dependent detection of polarization.

For the sake of simplifying the discussion, the three pulses involved in the experiment are modeled as δ functions in time. The electric field can then be described as

$$\vec{E}(t) = (\delta(t + t_1 + t_2)e^{i\phi_1}\, e^{i\mathbf{k_1}\cdot\mathbf{r}} + \delta(t + t_1)e^{i\phi_2}\, e^{i\mathbf{k_2}\cdot\mathbf{r}} + \delta(t)e^{i\phi_2}\, e^{i\mathbf{k_3}\cdot\mathbf{r}})\, e^{-i\Omega_L t} + c.c. \quad (26)$$

where t_1 and t_2 are the first and second time delays, respectively. The three pulses have a definite phase relationship between them described as ϕ_1, ϕ_2, and ϕ_3. Although the directional vectors **k** are labeled, in the phase cycling procedure, the directional vectors do not affect the experiment, since the pulses were chosen to be collinear.

Those terms that survive after the phase cycling process for our 2-D experiment (as described in section 4.1), i.e. rows 33−36 in Table 1, arise from a fourth order term in the density matrix expression. For instance, for row 34 (a cross-peak corresponding to (ω_a, ω_b)), the relevant element from the fourth order density matrix instantly after the last pulse (the excited-state population where the detectable fluorescence arises from) is[32]

$$\begin{aligned}\rho_{bb}^{(4)}(t=0) \propto \int\int\int\int d\tau_1\, d\tau_2\, d\tau_3\, d\tau_4 \times \\ \delta(t_1+t_2-\tau_1-\tau_2-\tau_3-\tau_4)\, e^{i\phi_1}\, e^{i\mathbf{k_1}\cdot\mathbf{r}}\, e^{-i\Omega_L(-\tau_4-\tau_3-\tau_2-\tau_1)} \times \\ \delta(t_2-\tau_2-\tau_3-\tau_4)\, e^{-i\phi_2}\, e^{-i\mathbf{k_2}\cdot\mathbf{r}}\, e^{i\Omega_L(-\tau_4-\tau_3-\tau_2)} \times \\ \delta(t_2-\tau_3-\tau_4)\, e^{i\phi_2}\, e^{i\mathbf{k_2}\cdot\mathbf{r}}\, e^{-i\Omega_L(-\tau_4-\tau_3)} \times \\ \delta(-\tau_4)\, e^{-i\phi_3}\, e^{-i\mathbf{k_3}\cdot\mathbf{r}}\, e^{-i\Omega_L(-\tau_4)}\, e^{-i\Omega_{ag}\tau_1}\, e^{-\Gamma_{ag}\tau_1} \times \\ e^{-i\Omega_{gg}\tau_2}\, e^{-\Gamma_{gg}\tau_2}\, e^{-i\Omega_{bg}\tau_3}\, e^{-\Gamma_{bg}\tau_3}\, e^{-i\Omega_{bb}\tau_4}\, e^{-\Gamma_{bb}\tau_4} \\ = e^{i\phi_1}\, e^{i\mathbf{k_1}\cdot\mathbf{r}}\, e^{-i\phi_3}\, e^{-i\mathbf{k_3}\cdot\mathbf{r}}\, e^{-i\omega_a t_1}\, e^{-i\omega_b t_2}\, e^{-\Gamma_{ag} t_1}\, e^{-\Gamma_{bg} t_2} \quad (27)\end{aligned}$$

where Ω_L is the laser center frequency and the other Ω's and Γ_{eg}'s are the frequency and generic decay constants, respectively, of the coherences. $\omega_a = \Omega_{ag} - \Omega_L$ and $\omega_b = \Omega_{bg} - \Omega_L$. The Feynman diagram for the process described in eq 27 is given in Figure 8. As is apparent from eq 27, the use of phases to label the interaction on this double-sided Feynman diagram serves the same purpose as the directional **k** vectors that are more commonly used.

Thus, by detecting excited-state population via the measurement of fluorescence, we are in fact detecting the sum of all possible directional components of the polarization. All possible quantum-coherence pathways (or Liouville-space pathways) are detected simultaneously in this experiment. The phase-cycling scheme serves to select one particular Liouville-space pathway.

5. Combining the Best of Both Worlds

Pulse phase control plays three major roles in NMR pulse sequence design: it permits coherence pathway selection, modification of the effective Hamiltonian, and heterodyne detection. For optical samples much longer than λ along the propagation direction, coherence pathway selection can also be achieved by directional detection with non-collinear pulses. In NMR the transverse magnetization does not produce a propagating electromagnetic field, so directional detection is not useful.

For example, the photon echo is the optical analogue of the spin echo. In a NMR spin echo with nonperfect pulses, $((90 + \delta)_x - t_1 - (180 + \epsilon)_x - t_2)$, there is also a free induction decay after the second pulse, and if the delay is short, there might also be some residual FID signal from the first pulse which survives the second pulse. In the perturbation picture, both of these are the first order processes; for example, the first FID reflects interaction with the first light pulse but not the second. These processes give rise to additional frequency components which could be suppressed by phase cycling in NMR. As was recognized long ago in optics, these imperfections are missing in the non-collinear laser experiment. The detection of (for example) the photon-echo signal at $2\mathbf{k}_2 - \mathbf{k}_1$ only picks out the component that evolves as a +1-quantum coherence during the first period and as a −1-quantum coherence during the second period. For linear operators in the Hamiltonian (for example, local variation in the resonance frequency due to lattice imperfections) the frequency shift on the −1-quantum and +1-quantum transitions are identical, so the sum of the two evolutions causes a refocusing (the echo).

However, directional variation is not as versatile as phase control. Directional variation forces an averaging over all possible phase relations. As long as the desired coherence is only phase-modulated by phase shifts, this simply creates a new spatial direction for the dipoles to reinforce. Thus, for example, the magnitude of the photon echo is unaffected by the relative phase of the two laser pulses. However, in general photon echoes do not remove all "inhomogeneous broadening". Consider, for example, a four level system consisting of the fundamental transitions of two different C═O stretches in an ensemble of molecules with different conformations. At any instant the angle and separation between the two transition dipoles vary across the ensemble, as does the magnitude of the coupling matrix element. This physical inhomogeneity would cause apparent dephasing of the macroscopic polarization after a single pulse, but this is a bilinear interaction which is not refocused by a photon echo.[33] Mathematically, taking either of the allowed transitions and reversing all of the state labels (as would happen with a π pulse) still changes a +1-quantum transition into a −1-quantum transition, but the frequency of the transition changes.

Such broadening mechanisms can be reversed, but only by pulses with a well-defined phase relation across the entire

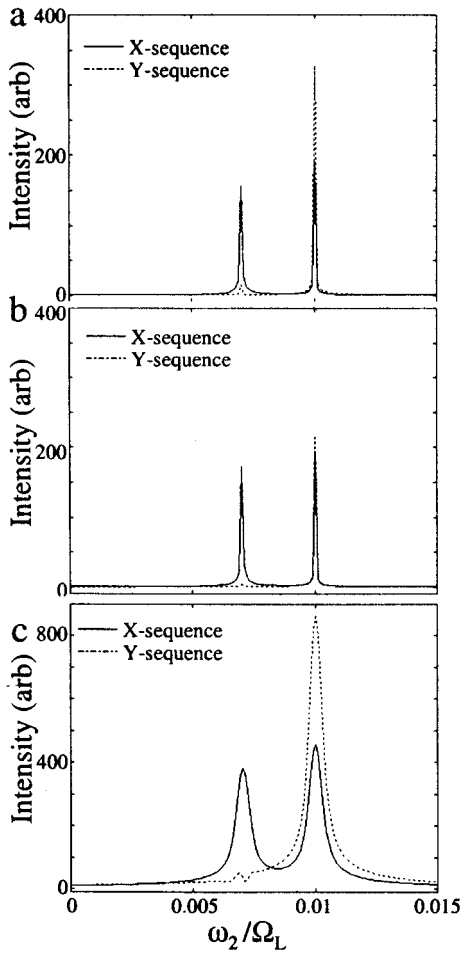

Figure 9. Elimination of selected transition using pulse sequences given in eqs 28 and 29. (a) Fourier transformation of the fluorescence signal as a function of t_2 with a fixed value of t_1. Using the *Y*-sequence, the transition at $\omega_2 = 0.007\Omega_L$ has a minimum intensity for $t_1 = 174$ fs for a pulse with an area of 0.4π. With the *X*-sequence this peak is clearly visible. (b) The same measurement as in a, but with a Gaussian intensity distribution with a peak area of 0.4π. In this case the peak at $\omega_2 = 0.007\Omega_L$ has a minimum intensity for the *Y*-sequence with $t_1 = 182$ fs. (c) The same measurement as in a, but with inhomogeneously broadened transitions. If the system is inhomogeneously broadened, the peak can still be eliminated with $t_1 = 174$ fs, if the individual peaks are well-separated.

sample. Consider two pulse-sequences given in eqs 28 and 29

X-sequence:

$$XXX - XX\bar{X} - iXXY - iXX\bar{Y} \tag{28}$$

Y-sequence:

$$XYX - XY\bar{X} - iXYY - iXY\bar{Y} \tag{29}$$

For a two-level system, it is possible to choose the delay between the first and the second pulse, t_1, in such a way that the second *X*-pulse will return the pseudo-spin vector exactly back along the *z*-axis. If that is the case, the phase cycling of the third pulse will result in no signal at all. At that same delay, the *Y*-sequence will still give a signal, since the *Y*-pulse will not return the polarization along the *z*-axis.

This effect is illustrated in Figure 9a, for the three level system discussed in Figure 2. The Fourier transformation with respect to t_2 of the fluorescence signal is plotted. The value of t_1 was fixed at 174 fs. The area of the pulse (on-resonance) was 0.4 π, and the pulse length is again 100 fs. It can be seen that, for the *Y*-sequence, the peak for the low-frequency transition is almost completely eliminated. For the *X*-sequence, both peaks are present. In the case of a two-level system, the low-frequency peak would have been eliminated completely at $t_1 = 173$ fs. In this case this peak cannot be completely eliminated, because of the coupling between the two transitions. However, it can be minimized at a t_1 close to the expected value. In Figure 9b, the calculation was repeated with a Gaussian intensity distribution, having a maximum area of 0.4 π. Since both transitions in this example are off-resonant, the time t_1 for which the peak is eliminated depends on the intensity of the laser. However, as can be seen from this figure, the peak can still be greatly reduced if a value of $t_1 = 182$ fs is used. Finally, in Figure 9c it is shown that also if the peaks are inhomogeneously broadenend, they can still be eliminated. In this case, t_1 was chosen as 174 fs again. Thus, by switching between *X* and *Y* pulses for a fixed delay t_1 and phase cycling the last pulse, one can switch a transition on and off. More generally, the $90_x - 90_y$ combination on resonance is the simplest pulse sequence which refocuses bilinear interactions (it is known as the "quadrupolar echo" because of its use in spin-1 systems, which are mathematically quite similar to the case illustrated here). In any system with bilinear couplings it produces a quite different state than does $90_x - 90_x$ and thus could be used to measure dipolar interactions (and their fluctuations, which would not be refocused).

6. Conclusion

In this paper we have proposed a technique to detect the time-dependent polarization introduced into a sample by the action of two pulses delayed by a time t_1. At time t_2 after the second pulse, a third pulse is applied which will partly convert the polarization into a population. This population is then detected by collecting the fluorescence from the sample. With this technique, couplings between transitions in the system can be detected through the presence of cross-terms in the two-dimensional spectrum. Additional, unwanted cross-peaks arise from nonperfect pulse areas, simultaneous excitation of two transitions, and negative frequency components, but it has been shown that a phase-cycling scheme can simplify these spectra tremendously. With current pulse shaping techniques, it has become straightforward to create the three delayed pulses with a phase independent of their delay that are needed for such experiments. Model calculations have shown that a sequence of experiments where the phases of the second and third pulses are rotated can eliminate all DC components and the negative frequency components.

As noted earlier, COSY and NOESY experiments in NMR only give information that is also available from double-resonance techniques; they merely present the information in a more convenient form. Similarly, two-dimensional optical COSY experiments (either the two-pulse experiment with heterodyne detection or the three-pulse experiments discussed here) are not necessarily better than dual-frequency pump−probe experiments. The situation changes if we adapt the model two-dimensional experiment (Figure 1) to include *directional variation between the preparation sequence and the mixing sequence* but limit the variation in either sequence individually. For example, suppose all the preparation pulses have wave vector $\mathbf{k}_p$ and the mixing pulses have wave vector $\mathbf{k}_m$. Now, for example, the preparation sequence can be designed with delays which select for a specific coupling magnitude, or refocus couplings over some range, and detection in the direction $2\mathbf{k}_m - \mathbf{k}_p$ restricts the detected signal to a specific coherence

pathway. The final role of the pulse phase is heterodyne detection. As Hybl and co-workers have shown,[8] this can be done in a straightforward way with multiple laser pulses and variations in direction, but transformation to the rotating frame is then quite difficult because pulse delay and pulse phase are intimately coupled. Here we suggest taking advantage of what is normally seen as a weakness of the spatial pulse shaping methods—beam translation proportional to delay.[34] With one more lens, this becomes an angular variation which remains coherent in the apparatus as the delay is increased.

More generally, then, we conclude that pulse direction variation, which has long been a stable of coherent optical pulse sequences, is equivalent to pulse phase control only for very simple sequences. Control of both simultaneously for femtosecond pulse sequences, which is only now technologically possible, has significant advantages and may open up a new generation of optical techniques.

Acknowledgment. This research was supported by the Air Force Office of Scientific Research and the Center for Ultrafast Laser Applications. The authors would like to thank D. Jonas for kindly providing us with a preprint of ref 9. Valuable discussions with Jeff Barnes and Jennifer Davis are greatly appreciated.

References and Notes

(1) Hahn, E. L. *Phys. Rev.* **1950**, *77*, 297.

(2) Feynman, R. P.; Vernon, F. L., Jr.; Hellwarth, R. W. *J. Appl. Phys.* **1957**, *28*, 49.

(3) Kurnit, N. A.; Abella, I. D.; Hartmann, H. R. *Phys. Rev. Lett.* **1964**, *13*, 567.

(4) Elsaesser, T.; Fujimoto, J. G.; Wiersma, D. A.; Zinth, W., Eds. *Ultrafast Phenomena XI*; Springer Verlag: Berlin, 1998.

(5) (a) Weiner, A. M. *Prog. Quantum Electron.* **1995**, *19*, 161. (b) Hillegas, C. W.; Tull, J. X.; Goswami, D.; Strickland, D.; Warren, W. S. *Opt. Lett.* **1994**, *9*, 737.

(6) (a) Kane, D. J.; Trebino, R. *IEEE J. Quantum Electron.* **1993**, *29*, 571. (b) Rhee, J.-K.; Sosnowski, T. S.; Tien, A.-C.; Norris, T. B. *J. Opt. Soc. Am. B* **1996**, *13*, 1780. (c) Iaconis, C.; Wong, V.; Walmsley, V. *IEEE J. Sel. Top. Quantum Electron.* **1998**, *4*, 285.

(7) Ernst, R. R.; Bodenhausen, G.; Wokaun, A. *Principles of Nuclear Magnetic Resonance in One and Two Dimensions*; Clarendon Press: Oxford, U.K., 1987.

(8) Hybl, J. D.; Albrecht, A. W.; Gallagher Faeder, S. M.; Jonas, D. M. *Chem. Phys. Lett.* **1998**, *297*, 307.

(9) Albrecht, A. W.; Hybl, J. D.; Gallagher Faeder, S. M.; Jonas, D. M. *J. Chem. Phys.*, to be submitted for published.

(10) Warren, W. S.; Silver, M. *Adv. Magn. Res.* **1988**, *12*, 248.

(11) Glaser, S. J.; Schulte-Herbruggen, T.; Sieveking, M.; Schedletzky, O.; Nielsen, N. C.; Sorensen, O.W.; Griesinger, C. *Science* **1998**, *280*, 421.

(12) Slichter, C. P. *Principles of Magnetic Resonance*, 3rd ed.; Springer-Verlag: Berlin, Heidelberg, 1990.

(13) (a) Aue, W. P.; Bartholdi, E.; Ernst, R. R. *J. Chem. Phys.* **1976**, *64*, 2229. (b) Weitekamp, D. *Adv. Mag. Res.* **1983**, *11*, 111. (c) Munowitz, M.; Pines, A. *Science* **1986**, *233*, 525.

(14) Wüthrich, K. *NMR of proteins and nucleic acids*; Wiley: New York, 1986.

(15) Freeman, R. *Bull. Magn. Reson.* **1986**, *8*, 120.

(16) (a) Carr, H. Y.; Purcell, E. M. *Phys. Rev.* **1954**, *94*, 6881. (b) Meiboom, S.; Gill, D. *Rev. Sci. Instrum.* **1966**, *16*, 1097.

(17) (a) Fetterman, M. R.; Goswami, D.; Keusters, D.; Yang, W.; Rhee, J. K.; Warren, W. S. *Opt. Express* **1998**, *3*, 366. (b) Hillegas, C. W.; Tull, J. X.; Goswami, D.; Strickland, D.; Warren, W. S. *Opt. Lett.* **1994**, *9*, 737. (c) Assion, A.; Baumert, T.; Bergt, M.; Brixner, T.; Kiefer, B.; Seyfried, V.; Strehle, M.; Gerber, G. *Science* **1998**, *282*, 919. (d) Weinacht, T. C.; Ahn, J.; Bucksbaum, P. H. *Phys. Rev. Lett.* **1998**, *80*, 5506. (e) Efimov, A.; Moores, M. D.; Beach, N. M.; Krause, J. L.; Reitze, D. H. *Opt. Lett.* **1998** *23*, 1915.

(18) Gordon R. J.; Rice, S. A. *Annu. Rev. Phys. Chem.* **1997**, *48*, 601.

(19) Allen, L.; Eberly, J. H. *Optical Resonance and Two-Level Atoms*; Wiley: New York, 1975.

(20) (a) Lee, S.; Richter, W.; Vathyam, S.; Warren, W. S. *J. Chem. Phys.* **1996**, *105*, 874. (b) Warren, W. S.; Richter, W.; Andreotti, A. H.; Farmer, S. *Science* **1993**, *262*, 2005.

(21) Hecht, E. *Optics*, 3rd ed.; Addison-Wesley: Reading, MA, 1998.

(22) Orlowski, T. E.; Jones, K. E.; Zewail, A. H. *Chem. Phys. Lett.* **1978**, *54*, 197.

(23) Yang, W.; Keusters, D.; Goswami, D.; Warren, W. S. *Opt. Lett.* **1998**, *23*, 1843.

(24) (a) Abella, I. D.; Kurnit, N. A.; Hartmann, S. R. *Phys. Rev.* **1966**, *141*, 391. (b) Bai, Y. S.; Fayer, M. D. *Chem. Phys.* **1988**, *128*, 135.

(25) Leibfried, D.; Meekhof, D. M.; King, B. E.; Monroe, C.; Itano, W. M.; Wineland, D. J. *Phys. Rev. Lett.* **1996**, *77*, 1796.

(26) Warren, W. S.; Zewail, A. H. *J. Chem. Phys.* **1981**, *75*, 5856.

(27) Spano, F.; Haner, M.; Warren, W. S. *Chem. Phys. Lett.* **1987**, *135*, 97.

(28) Cho, M.; Scherer, N. F.; Fleming, G. R.; Mukamel, S. *J. Chem. Phys.* **1992**, *96*, 5618.

(29) Zhang, W. M.; Chernyak, V.; Mukamel, S. *J. Chem. Phys.* **1999**, *110*, 5011.

(30) Sundström, V.; Gillbro, T. *J. Chem. Phys.* **1985**, *83*, 2733.

(31) Hamm, P.; Lim, M.; Hochstrasser, R. M. *J. Phys. Chem. B* **1998**, *102*, 6123.

(32) Mukamel, S. *Principles of Nonlinear Optical Spectroscopy*; Oxford University Press: New York, 1995.

(33) Warren, W. S.; Zewail, A. H. *J. Phys. Chem.* **1981**, *85*, 2309.

(34) (a) Wefers, M. M.; Nelson, K. A.; Weiner, A. M. *Opt. Lett.* **1996**, *21*, 746. (b) Tull, J. X.; Dugan, M. A.; Warren, W. S. *Adv. Magn. Opt. Reson.* **1997**, *20*, 1.